ACI MATERIALS JOURNAL TECHNICAL PAPER

MS No. M-2013-023.R2

Feasibility Study on Fire-Resistive Engineered Cementitious Composites

by Qian Zhang, Ravi Ranade, and Victor C. Li

Spray-applied fire-resistive material (SFRM) is one of the most commonly used fire protection materials for steel structures. The commonly observed delamination and detachment of SFRM, however, significantly reduces the overall effectiveness of fire protection. Engineered cementitious composites (ECCs) are a special family of high-performance, fiber-reinforced cementitious composites featuring very high ductility under tension, bending, and impact loads. This study investigates the feasibility of developing a new version of fire-resistive ECC that combines the fracture-resistant property of the ECC family of materials and the excellent insulation property of SFRM. The study shows that ECC with similar or even better insulation property compared with conventional SFRM can be developed, and the intrinsic high ductility of ECC improves the overall effectiveness and durability of fire protection.

Keywords: ductility; durability; engineered cementitious composite; impact; spray-applied fire-resistive material; thermal conductivity.

INTRODUCTION

Spray-applied fire-resistive materials (SFRMs) are commonly used for fireproofing structural steel. There are two major types of SFRM commercially available in the market: cementitious (wet-mix) and mineral-fiber-based (dry-mix). Cementitious SFRMs are lightweight gypsum or portland cement-based plasters containing a large volume of lightweight fillers that are premixed with water (hence called wet-mix) and sprayed on the steel substrate. SFRMs are also divided into three categories based on their dry density: standard density (208 to 288 kg/m^3 [13 to 18 lb/ft^3]), medium density (352 to 480 kg/m^3 [22 to 30 lb/ft^3]), and high density (over 640 kg/m^3 [40 lb/ft^3]) SFRM. Higher-density SFRMs typically possess better strength and durability than lower-density SFRMs. Most commercial SFRMs, particularly medium- and high-density SFRMs, are cementitious materials that use portland cement as binder. Fire protection offered by SFRM is mainly due to its excellent insulation (low thermal conductivity), which substantially delays the temperature rise in the structural steel. The many advantages offered by SFRM, mainly low thermal conductivity, light self-weight, cost-efficiency, and ease of application, make it a widely-used fire protection material in the United States and Canada.[1]

The performance of SFRM coated on steel members, however, depends not only on its thermal properties, but also the durability properties of SFRM during the service life of a structure.[2] The term "durability" in this paper refers to the ability of SFRM to stay intact on the steel substrate. SFRM durability is often called into question even under normal service loads due to its brittleness and poor bond with steel.[3] This problem is further exacerbated under accidental actions (such as impact caused by installation or construction work after SFRM has been applied), earthquakes, or man-made hazards.[4,5] In such events, the spray-on fireproofing material may detach or delaminate from the steel members. The loss of insulation significantly reduces the effectiveness of the fire protection under such extreme load/displacement/thermal events.[6-8] In spite of the satisfactory insulation properties of SFRM, their functional performance to protect steel structures is limited by inherent brittleness and poor bond with steel.

The integrity of SFRM protected steel member is limited by potential adhesive failure at the SFRM/steel interface, cohesive failure of the SFRM within the material, or both. While adhesive failure reflects a deficiency in interfacial bonding property between steel and SFRM, cohesive failure is intrinsically associated with the low material tensile strength and brittleness. The tensile strength of a common medium density (352 to 480 kg/m^3 [22 to 30 lb/ft^3]) SFRM material is below 0.1 MPa (14.5 psi),[3] and the fracture toughness of SFRM (not reported in literature) is expected to be substantially less than normal concrete, that is, less than 0.2 MPa$\sqrt{m}$ (182.0 psi$\sqrt{in.}$). This makes SFRM prone to cracking even under service loads. Because SFRM is often loaded via imposed displacement (for example, due to differential thermal movement between SFRM and steel), another important tensile property of SFRM is the tensile strain capacity. Although there is no documented tensile strain capacity data on SFRM in the literature, it should be comparable to or less than that of normal concrete (approximately 0.01%). For such material, the durability of the fire-protected steel member significantly relies on the interface adhesive strength, which has been shown to be insufficient to prevent dislodgement of SFRM under impact or monotonic load.[3] It is recognized that the lack of resistance to adhesive and cohesive failures is a major shortcoming of current SFRM.[9]

Engineered cementitious composites (ECCs), a special family of ultra-ductile, high-performance fiber-reinforced cementitious composites, is a plausible solution for the problem described previously. ECC has been developed based on micromechanics principles[10-12] over the last decade

ACI Materials Journal, V. 111, No. 1-6, January-December 2014.

as a ductile construction material alternative to conventional concrete. Its tensile strain capacity under uniaxial tension reaches 3 to 5%, approximately 300 to 500 times that of normal concrete.[13,14] Under tensile load, ECC develops multiple microcracks instead of one large crack, and the load-carrying capacity continues to increase after first crack, thus achieving pseudo strain-hardening behavior. This damage-tolerant feature and large deformation capacity of ECC can be beneficial for deformation compatibility with the steel substrate under mechanical loading, thermal loading, or both. An added benefit is that the micro-sized cracks in ECC (typically 30 to 50 μm [0.00118 to 0.00197 in.] wide), compared with millimeter size cracks in SFRM and other brittle cement-based materials, can potentially cause less heat transfer through radiation via crack openings under high temperature. Due to the desirable properties of tensile ductility, damage tolerance, and small crack widths, ECC can be potentially developed as safer insulation alternative to SFRM for protecting steel structures from heat-related failures, which is the motivation behind this study.

ECC can be designed to have different functions for various applications. For example, in previous studies, lightweight ECC[15] with density (wet-density) as low as 900 kg/m^3 (56.2 lb/ft^3), and sprayable ECC[16] designed to be applied by a pump and spray process were developed following the micromechanics-based design approach. In this study, an essential objective is to endow ductile ECC with good thermal insulating property.

Another aspect of ECC relevant to the present research for a new generation of fire insulation material is its ability to withstand impact loading. It was demonstrated that by micromechanics based tailoring of fiber, matrix, and particularly the fiber/matrix interface, tensile ductility of ECC can be maintained even under high rate loads.[17] Impact resistance of ECC is useful to preventing damage to the fire-resistive material during a structure's service life and extreme loading events.

In spite of the desirable characteristics of ECC discussed above, it has never been investigated as a fire-resistive material. Past research on ECC behavior (for example, thermal shock[18] and spall resistance[19]) suggests advantages of ECC under thermal loading. To the best of the authors' knowledge, no study has been conducted to characterize the thermal conductivity of ECC under elevated temperature. The effects of the mechanical performance (both ductility and impact resistance) of ECC on the durability of the fireproofing system should also be investigated for implementation in steel structural applications. This research aims to fill this gap of knowledge by demonstrating the feasibility of developing ECC as a fire-resistive material with desired thermal and mechanical properties.

In this feasibility study, a preliminary mixture proportion of fire-resistive ECC (FR-ECC) is presented. The thermal insulation property (thermal conductivity) of FR-ECC is characterized in accordance with the test procedures of ASTM E2584.[20] The mechanical behavior of FR-ECC is characterized by direct uniaxial tension and compression tests. Low-velocity impact tests are carried out on FR-ECC coated steel panels to evaluate the durability of the material under impact load. In addition, because of the high cohesive strength and damage tolerance of ECC, a new durability concept of wrapped-around durability is introduced. Wrapped-around durability refers to fully wrapping a highly ductile and strong insulation material around a steel member. The integrity of this fire-protection system relies solely on the cohesion property of the insulation material, with almost no dependence on the adhesion between the insulation material and steel substrate. In this study, validity of this concept is demonstrated by low-velocity impact tests. Test results and findings are documented in this paper.

RESEARCH SIGNIFICANCE

A new material for thermal insulation of steel, FR-ECC, is proposed in this research to overcome the durability (ability of SFRM to stay on the steel substrate) bottleneck of currently used SFRMs. Although ECC has been extensively studied for a variety of structural and durability applications, it has never been investigated as a fire-protection material before. This study demonstrates the feasibility of developing FR-ECC with desired thermal and mechanical properties (ductility and impact resistance) through a micromechanics-based design approach. A novel idea of wrapped-around durability of FR-ECC is also illustrated in this study. This research lays out the scientific foundation for continued development and investigation of FR-ECC, which has the potential to substantially reduce the risk of fire-related failures in steel structures.

EXPERIMENTAL INVESTIGATION

Material design considerations

In this feasibility study, the objectives of the material design of FR-ECC are to achieve good insulation property and ductile mechanical performance (strain capacity > 2%) simultaneously in one material for the targeted application. The desired thermal insulating property of FR-ECC is very low thermal conductivity of the material, similar to or less than that of conventional SFRM, so that it delays the temperature rise of steel under fire. Typical thermal conductivity of a conventional SFRM is 0.05 to 0.32 W/(m·K) (0.029 to 0.185 BTU·h^{-1}/[ft·F]) within the temperature range of 20 to 650°C (68 to 1202°F) measured in the authors' laboratory in accordance with ASTM E2584.[20] Without any modification, the thermal conductivity of a frequently studied ECC (M45) is 0.15 to 0.63 W/(m·K) (0.087 to 0.364 BTU·h^{-1}/[ft·F]) within the same temperature range. In addition to low thermal conductivity, ductile mechanical performance of FR-ECC is required, which is achieved by following the micromechanics-based design principles.[10-12]

Thermal conductivity is closely associated with the microstructure, particularly pore structure, of the material. It is known that the thermal conductivity decreases with increase in total porosity of the material[21-26] due to the fact that air has significantly lower thermal conductivity compared with solid and liquid phases. As the total porosity is closely related to bulk density, the thermal conductivity of concrete often decreases with decrease in bulk density.[27-29] In addition to porosity, pore size distribution is also important for

Table 1—Mixture proportion of FR-ECC

Cement (C), kg/m^3 (lb/yd^3)	419.6 (707.3)
Water (W), kg/m^3 (lb/yd^3)	314.7 (530.4)
S38 glass bubbles (GB), kg/m^3 (lb/yd^3)	209.8 (353.6)
Fiber,* kg/m^3 (lb/yd^3)	26 (43.8)
High-range water-reducing admixture (SP), kg/m^3 (lb/yd^3)	12.6 (21.2)
Viscosity-modifying admixture (VMA), kg/m^3 (lb/yd^3)	21.0 (35.4)

*Polyvinyl alcohol (PVA) fiber of 12 mm (0.5 in.) length and 0.3% oil coating used.

Table 2—Physical properties of 3M S38 glass bubbles

Density, kg/m^3 (lb/yd^3)	380 (640.5)
Composition	Soda-lime-borosilicate glass
Average diameter, μm (in.)	40 (0.002)
Effective maximum diameter, μm (in.)	85 (0.003)
Isostatic crush strength, MPa (psi)	27.6 (4000)
Softening point, °C (°F)	600 (1112)

high temperature applications.[25,26,30] Heat transfer theory predicts that the equivalent thermal conductivity of a pore due to radiation is proportional to pore size. The apparent thermal conductivity equals the sum of true conductivity due to conduction and equivalent conductivity due to radiation. Hence, to attain low thermal conductivity at high temperature, it is desirable to have high porosity and small pore size.

To reach the targeted low thermal conductivity in cementitious insulation materials, a widely used technique is to add lightweight porous aggregates, such as expanded perlite and vermiculite, in the matrix. For choosing a suitable lightweight aggregate for FR-ECC with desired composite properties, the following considerations are important: 1) air void size inside the aggregate is minimized to reduce the radiation heat transfer effect; and 2) aggregate size is preferably smaller than 1 mm (0.0394 in.), and with smooth shape to reduce adverse effects on the mechanical performance of ECC.

Strain-hardening behavior of ECC under tension is achieved by the formation of multiple microcracks after initial cracking of the matrix. For achieving multiple microcracks, the ECC microstructure should be tailored to satisfy the following strength and energy criteria (Eq. (1) and (2)).[10,11,31]

$$\text{energy-based criterion: } J_{tip} \le \sigma_0\delta_0 - \int_0^{\delta_0}\sigma(\delta)d\delta \equiv J_b' \quad (1)$$

$$\text{strength-based criterion: } \sigma_0 > \sigma_{cs} \quad (2)$$

where σ_0 is the maximum bridging stress corresponding to the crack opening δ_0; σ_{cs} is the cracking strength of the matrix; J_{tip} is the fracture energy of the matrix, which is approximately equal to K^2_m/E_m, where K_m is the matrix fracture toughness and E_m is the matrix Young's modulus. Equation (1) describes the energy balance in the crack extension process. Failure to meet this criterion results in the Griffith crack mode with unrestricted crack width as the crack extends.[32] The composite ingredients should be tailored to achieve sufficient margin between complimentary energy of fiber bridging J_b' and crack tip toughness J_{tip} to enable saturated multiple cracking and robust tensile ductility.[14,33] This requires limiting the matrix fracture toughness (that limits J_{tip}) and/or increasing J_b' by adjusting fiber properties (volume fraction, length, diameter, tensile strength, and modulus) and fiber/matrix interfacial properties (fiber/matrix frictional and chemical bonds). Equation (2) describes the strength criterion of multiple cracking, which requires the fiber bridging strength to be higher than the matrix cracking strength that is a function of the matrix defect size. If either inequality (Eq. (1) or (2)) is not satisfied, the composite fails with a single localized fracture, instead of multiple cracking, and a typical tension-softening behavior of normal fiber-reinforced concrete is observed.

In a previous study,[15] micron-sized hollow glass bubbles were successfully used to produce lightweight ECC material with mechanical properties (compressive strength and tensile ductility) suitable for structural applications. The average size of these micro glass bubbles is 20 to 40 microns (0.00079 to 0.00157 in.). Unlike other angular lightweight aggregates, these tiny spherical glass bubbles have less resistance to crack propagation that lowers the matrix fracture toughness in favor of satisfying the strain-hardening criterion (Eq. (1)). In addition to the benefit of enhancing tensile ductility of ECC, hollow glass bubbles are thermally stable up to very high temperature (600°C [1112°F]). A thermal gravimetric analysis (TGA) (Fig. A1 in the Appendix*) of the glass bubbles conducted by the authors shows that the weight reduction is less than 1% over the temperature range of 20 to 800°C (68 to 1472°F). Therefore, the glass bubbles are expected to be stable at a high temperature, and the size of entrapped air voids in these bubbles will be maintained at micron size up to a very high temperature. As previously discussed, this is beneficial in maintaining low equivalent thermal conductivity (due to radiation) at a high temperature. Thus, lightweight ECC made with these glass bubbles as aggregates seems a suitable candidate for FR-ECC.

One version of lightweight ECC (Table 1) containing a large volume fraction of 3M S38 glass bubbles is selected as preliminary mixture proportion for FR-ECC in this study. The material properties of the glass bubbles and fibers used are listed in Tables 2 and 3, respectively. Micrographs from a scanning electron microscope (SEM) of the glass bubbles before and after mixing with the cementitious matrix are shown in Fig. 1. It can be seen in Fig. 1 that the micro glass bubbles are well dispersed within the matrix, and maintain their spherical shape with entrapped air inside. This indicates that the glass bubbles survive the mixing procedure and maintain their original microstructure as desired.

Mechanical properties characterization

The mechanical properties characterization of FR-ECC involved experimental determination of uniaxial compressive strength and direct tension behavior.

*The Appendix is available at **www.concrete.org/publications** in PDF format, appended to the online version of the published paper. It is also available in hard copy from ACI headquarters for a fee equal to the cost of reproduction plus handling at the time of the request.

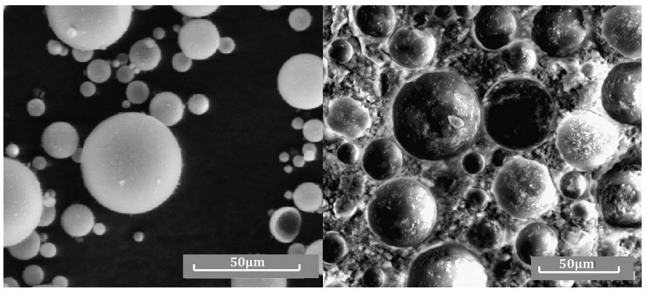

(a) (b)

Fig. 1—SEM images of glass bubbles: (a) before; and (b) after mixing procedure.

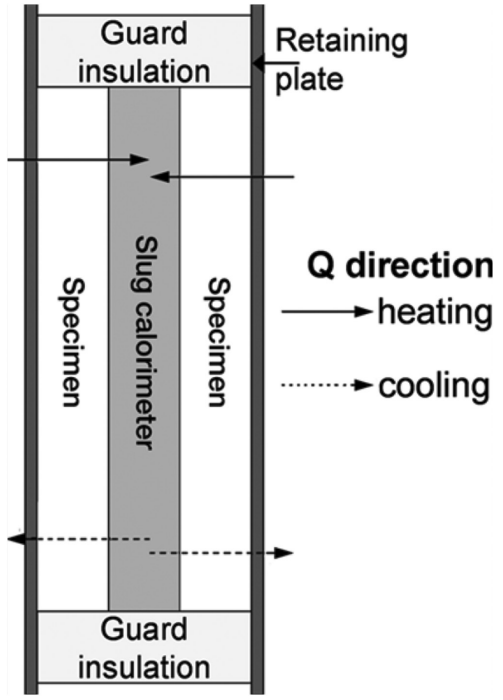

Fig. 2—Apparent thermal conductivity test setup.[18]

The compressive strength of FR-ECC was measured using a set of three 50.8 mm (2 in.) cube specimens. The test was conducted using a compression test system at a loading rate of 1300 ± 300 N/s (292 ± 68 lb/s) in accordance with ASTM C109.[34]

The direct tension tests were conducted using the uniaxial tension test setup (Fig. A2 in the Appendix) on a set of three specimens. The test involves loading a thin plate specimen of 203.2 mm (8 in.) long, 76.2 mm (3 in.) wide, and 12.7 mm (0.5 in.) thick. In this preliminary study, material was cast into the desired specimen configuration (as mentioned previously) instead of spraying. Before testing, four aluminum plates (76.2 x 50.8 mm [3 x 2 in.]) were glued to the four ends of the plate specimen to facilitate gripping. Tests were conducted on a test system with 100 kN (22 kip) capacity, under a displacement control at the rate of 0.5 mm/min (0.02 in./min) as recommended by Japan Society of Civil Engineers for direct tension testing of high-performance fiber-reinforced cementitious composites.[35] Two external linear variable differential transducers (LVDTs) were attached to the specimen edges, with a gauge length of approximately 101.6 mm (4 in.), to measure the tensile strain.

Table 3—Characteristics of PVA fiber

Nominal strength, MPa (ksi)	1620 (235)
Apparent strength, MPa (ksi)	1092 (158)
Diameter, μm (in.)	39 (0.002)
Length, mm (in.)	12 (0.5)
Young's modulus, GPa (ksi)	42.8 (6200)
Elongation, %	6.0
Density, kg/m^3 (lb/yd^3)	1300 (2190)
Melting temperature, °C (°F)	230 (446)

All specimens were tested at the age of 28 days after curing under laboratory room conditions (23 ± 3°C [73.4 ± 5.4°F]; 30 ± 10% relative humidity). The compressive strength and tensile stress-strain curve of the FR-ECC specimen were obtained using the aforementioned test setups.

Thermal property characterization

To assess the insulation property of FR-ECC, apparent thermal conductivity of the material was measured using a thermal capacitance calorimeter in accordance with ASTM E2584.[20] A high-density SFRM (with a density of 704 to 768 kg/m^3 [44 to 48 lb/ft^3]) commonly used in the United States was adopted as control to evaluate the performance of FR-ECC. The test configuration is shown in Fig. 2. The setup requires two plate specimens of insulation material (that is being tested) with dimensions of 152.4 x 152.4 x 25.4 mm (6 x 6 x 1 in.) sandwiching a stainless steel slug. Additional insulation material with very low thermal conductivity was used to cover all four edges of the specimen to enforce a one-dimensional heat transfer within the specimen. The assembled specimen was then placed in a small-scale furnace with maximum heating capacity up to 1000°C (1832°F), and heated up from room temperature to a critical temperature where the corresponding steel slug temperature reaches 537°C (999°F) (the temperature at which steel experiences substantial strength loss) at the rate of 5°C/min (9°F/min). The temperature of the slug (T_{slug}) and outer surface of the specimen ($T_{surface}$) were measured and recorded at a constant time interval of 1 minute using K-type thermocouples. After reaching the critical point, the test was aborted by shutting down the furnace, and the specimen was allowed to naturally cool down to room temperature. Two heating and cooling cycles were adopted for more reliable data.

The apparent thermal conductivity is calculated based on one-dimensional heat transfer analysis as

$$\lambda_a = \frac{FL(M^{SSS}C_p^{SSS} + M^{SPEC}C_p^{SPEC})}{2A\Delta T} \quad (3)$$

where λ_a is the apparent thermal conductivity; F is the measured heating rate within the slug (determined as the time derivative of T_{slug}); L is the thickness of the specimen; M^{SSS} and M^{SPEC} are the masses of steel slug and plate specimen of the insulation material being tested, respectively; C_P^{SSS}

and C_P^{SPEC} are their respective heat capacities—herein, heat capacity of the steel slug is determined using the expression $C_P^{SSS} = 6.683 + 0.04906 \times T + 80.74 \times \ln(T)$ (T in Kelvin); A is the area of the specimen perpendicular to the heat flow; and ΔT is the temperature gradient between the two surfaces of a plate specimen (determined as the difference between $T_{surface}$ and T_{slug}). Specific heat capacity (C_P^{SPEC} in Eq. (3)) of materials (FR-ECC and SFRM) was characterized using differential scanning calorimetry (DSC) in accordance with ASTM E1269.[36]

Cohesive property under impact load

Characterization of the cohesion of FR-ECC compared with conventional SFRM cover on steel substrate under impact load is evaluated in this part of the study. As pointed out previously, failure of the insulation cover can be due to lack of adhesion between insulation material and steel or lack of cohesion within the insulation material. This study focuses on comparing the cohesive behavior of FR-ECC and SFRM. The integrity of FR-ECC compared with conventional SFRM under impact loads was evaluated using a drop weight test (Fig. A3 in the Appendix) in terms of number of drops needed to detach the insulation cover from a steel substrate. Thin square steel panels with dimensions of 304.8 x 304.8 x 9.53 mm (12 x 12 x 0.375 in.) were used as steel substrates to emulate a real steel structural element. In this feasibility study, the FR-ECC was cast, instead of sprayed, on this steel substrate. A widely used type of commercial water-based bonding agent was applied on the substrates to enforce adequate bonding on the steel surface to deliberately force the damage to form within the material, thereby eliminating the possibility of adhesive failure. A control specimen with the same type of conventional high-density SFRM was also prepared and tested. One specimen for each type of insulation material (FR-ECC or SFRM) was tested for behavior characterization.

During the test, the steel substrate was simply supported on its edges (Fig. A4 in the Appendix). An impact test was performed using a drop weight of 8.91 kg (19.6 lb) with an impact head of 50.8 mm (2 in.) in diameter freely falling from a height of 1.17 m (46 in.) on the panel specimen (FR-ECC/SFRM). After each impact, the conditions of the FR-ECC and SFRM material were examined and photographically documented to qualitatively assess the integrity of the insulation cover.

Wrapped-around durability study

The damage tolerance of FR-ECC gives rise to a potentially new concept of wrapping a continuous layer of FR-ECC around the steel members, thereby eliminating the need for a strong adhesive strength at the steel-FR-ECC interface. The central idea is that if a structural steel member is continuously covered by FR-ECC (fully wrapped-around; refer to Fig. 3) that can maintain its continuity and integrity under mechanical and thermal loads, the integrity of the steel-FR-ECC system is ensured even when the bonding between steel and the FR-ECC (insulation) cover is lost. Thus, the wrapped-around durability concept provides an extra level of safeguard for steel members against fire, in addition to strong adhesive bonding between FR-ECC and steel.

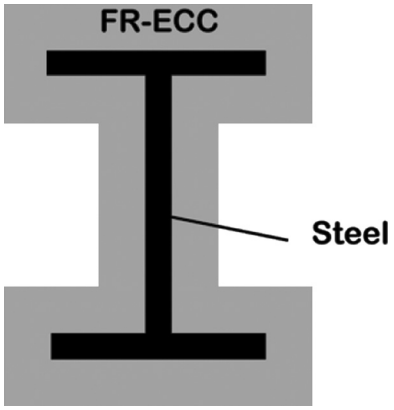

Fig. 3—Wrapped-around specimen configuration.

To evaluate the wrapped-around durability concept, low-velocity impact testing of a steel I-beam section fully wrapped with FR-ECC (and SFRM as control) was performed using the drop-weight test with an impact head of 50.8 mm (2 in.) in diameter. The wrapped-around durability is directly related to the impact resistance of the fire-proofing material (SFRM/FR-ECC). The beam specimens were prepared by applying an approximately 12.7 mm (0.5 in.) thick FR-ECC/SFRM layer on an S4 x 7.7 I-beam. The thickness of the fire-proofing materials was chosen based on common practice in the field. The beam was 609.6 mm (24 in.) long, and the fireproofing material was applied on the mid-406.4 mm (16 in.) length, leaving an approximately 101.6 mm (4 in.) space at each end for the simple support. For the FR-ECC specimen, an oil release agent was applied on the steel surface to deliberately create a totally bond-free interface between steel and FR-ECC to evaluate the integrity of the fire-proofing material with no bond with steel under impact loadings. In the control specimen made with SFRM, no oil release agent was used, and SFRM was naturally bonded to the steel surface. Impact tests consisting of four series of impacts were applied to the wrapped-around beam specimens. The drop weight, drop height, and number of impacts in each impact series are listed in Table 4. The drop weight test was designed to fail the specimen by gradually increasing the impact energy applied to the specimens, and the drop weights and heights were chosen considering the capacity of the drop weight tower. Examinations and photo documentations of the specimens were conducted after each impact to qualitatively evaluate the damage condition of the specimen.

EXPERIMENTAL RESULTS AND DISCUSSION

Mechanical properties

Compressive strength of FR-ECC at 28 days is measured to be 22.3 ± 3.3 MPa (3234.3 ± 478.6 psi). The compressive strength of FR-ECC surpasses the minimum strength specifications[37,38] for fire-proofing materials by an order of magnitude. The dry density of FR-ECC measured according to ASTM E605[39] is 857 kg/m^3 (53.5 lb/ft^3), which is compa-

Table 4—Impact details of durable wrap-around test

Impact series	No. of impacts	Drop weight, kg (lb)	Drop height, cm (in.)
1	3	5.05 (11.13)	86.36 (34)
2	3	7.31 (16.12)	86.36 (34)
3	3	7.31 (16.12)	111.76 (44)
4	6	8.91 (19.64)	111.76 (44)

rable to conventional high-density SFRM typically within the range of 640 to 1280 kg/m^3 (40 to 80 lb/ft^3).

The direct tension stress-strain relationship of FR-ECC is shown in Fig. 4. Robust strain-hardening behavior with tensile strain capacity exceeding 2% and tensile strength of over 2 MPa (290 psi) is observed, which is approximately two orders of magnitude larger than SFRM. The substantially higher tensile and compressive strengths of FR-ECC compared with SFRM improve the material's ability to withstand service loads. The high tensile ductility enables FR-ECC to accommodate large deformation of the steel substrate without delamination or detachment under impacts and other unexpected loads. The average residual crack width after unloading is approximately 15 μm (5.9×10^{-4} in.), measured using the procedure detailed in Li and Li.[40] The micro-sized cracks limit heat transfer associated with radiation compared with larger crack openings. Instead of one large crack and brittle failure in SFRM, multiple microcracks are formed in FR-ECC, maintaining integrity under increasing tensile load, and thus improving the overall durability of the fire protection system.

Thermal properties

The thermal conductivities, which directly relate to fireproofing abilities, of the two materials (FR-ECC and SFRM) are compared using the expression for one-dimensional conductivity in Eq. (3). The specific heat capacities of both the materials and masses of the plate specimens needed in Eq. (3) were experimentally determined.

The specific heat capacities of FR-ECC and SFRM (C_P^{SPEC} in Eq. (3)) were determined using DSC. Instead of treating the specific heat capacity as a temperature-dependent variable, the specific heat capacity measured at 400°C (752°F) for both materials was assumed constant throughout the entire temperature range (approximately 40 to 670°C [104 to 1238°F]) under investigation. This assumption is justified by previous research.[41] The measured specific heat capacities C_P^{SPEC} are 930 J/(kg·K) (0.222 BTU/[lb·F]) and 947 J/(kg·K) (0.226 BTU/[lb·F]) for FR-ECC and SFRM (control), respectively.

The mass of the specimen was considered as temperature-dependent in this study, as it varied considerably (for both FR-ECC and SFRM) before and after the thermal conductivity tests due to physical and chemical reactions (such as loss of moisture and decomposition of hydration product). During the thermal conductivity experiments, the mass loss is typically 15 to 30% after heating from room temperature (20°C [68°F]) up to approximately 700°C

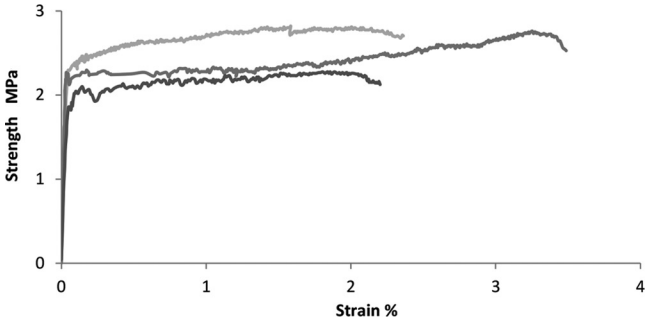

Fig. 4—Tensile stress-strain curves of FR-ECC. (Note: 1 MPa = 145 psi.)

(1292°F). Based on this observation, the mass of the specimen (M^{SPEC}) was assumed to be a linear function, as shown in Eq. (4)

$$M^{SPEC} = M_0 + \frac{M_f - M_0}{T_{max} - T_0}(T - T_0) \quad (4)$$

where M_0 and M_f are measured specimen mass before and after the test, respectively; and T_{max} and T_0 are the maximum specimen temperature during test and the initial room temperature before heating, respectively. The error caused by assuming that the mass loss is a linear function of temperature is expected to be insignificant because the $M^{SSS}C_P^{SSS}$ term is much larger than $M^{SPEC}C_P^{SPEC}$. The linear function of mass is used only in the heating phase of first heating and cooling cycle, and is assumed to be a constant during the cooling phase of the first cycle and entire second cycle. This assumption is reasonable because most of the physical and chemical changes associated with temperature are completed during the first heating phase.

The apparent thermal conductivity of FR-ECC and SFRM (control) specimens are subsequently determined by the temperature measurements on the outer surface of the specimen $T_{surface}$ and in the stainless slug T_{slug}. The apparent thermal conductivity, as a function of average specimen temperature (determined as the average of $T_{surface}$ and T_{slug}) within the heating phase of the first heating and cooling cycle, are plotted in Fig. 5. These curves are based on the test results of sets of three specimens for both FR-ECC and SFRM. The drop in apparent thermal conductivity in the first cycle is caused by a variety of physical and chemical reactions, such as evaporation of moisture and loss of physical bonded water, which delays the temperature rise. This phenomenon was not observed in the heating phase of the second cycle.

In Fig. 5, it is observed that, apart from a slightly higher averaged thermal conductivity of FR-ECC compared with SFRM between 180 and 240°C (356 and 464°F), FR-ECC exhibits a lower thermal conductivity compared with the control (SFRM) specimen over much of the temperature range investigated in this paper. With similar specific heat capacity and density, the lower thermal conductivity of FR-ECC indicates that the overall insulation property (ability to delay temperature rise in steel) of FR-ECC is generally better than the conventional SFRM used in this

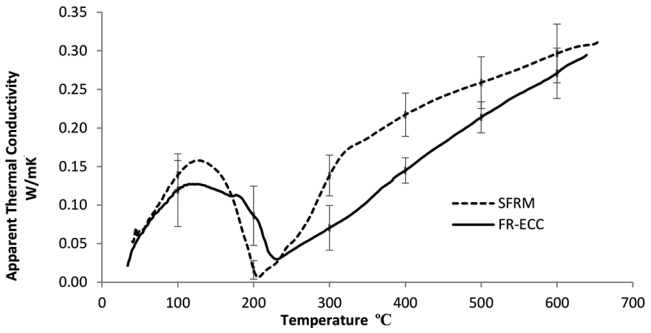

Fig. 5 –Measured apparent thermal conductivity of FR-ECC and conventional SFRM during the heating phase of Cycle 1. (Note: °C = (°F – 32) × 5/9; 1 W/mK = 0.578 BTU·h^{-1}/(ft·F).)

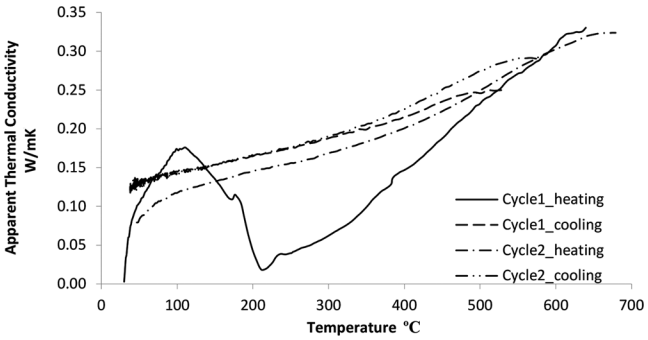

Fig. 6—Measured apparent thermal conductivity of FR-ECC during two consecutive heating and cooling cycles. (Note: °C = (°F – 32) × 5/9;1 W/mK = 0.578 BTU·h^{-1}/(ft·F).)

study over the major temperature range. The test results show that FR-ECC satisfies the thermal requirement as a fire-resistive material.

Figure 6 shows the apparent thermal conductivity of FR-ECC measured during two consecutive heating and cooling cycles. Other than the first heating cycle (reasons explained previously), the thermal conductivity shows a good consistency during both heating and cooling cycles. Because the thermal conductivity is mainly governed by the pore structure inside the material, this consistency may indicate that the pore structure is stable under multiple heating and cooling cycles. This observation also justifies using glass bubbles as lightweight aggregates, as they are very stable under elevated temperature and are able to maintain the pore structure as desired. The thermal insulation ability of FR-ECC over the heating cycles is considered satisfactory.

Cohesive property under impact load

The cohesive strengths of both fire-proofing materials (FR-ECC and SFRM) were evaluated experimentally using drop-weight impact tests on steel panel substrates covered with a fire-proofing material layer of thickness 25.4 mm (1 in.), which is a typical thickness in field construction, as detailed in the previous section. Figure 7 shows the contrast of the failure pattern in SFRM (after six successive impacts) and microcrack pattern (without failure) in the FR-ECC specimen after 12 successive impacts.

The material integrity was not preserved in the SFRM specimen, even with the presence of strong interfacial adhesion with steel substrate. After the first impact, no noticeable damage was observed in SFRM specimen. The SFRM, however, began to detach from the substrate after the second impact. Finally, after the sixth impact, most of the SFRM had detached, as shown in Fig. 7(a). Delamination occurred within a few millimeters near the interface, and large millimeter-sized radial cracks formed due to the tensile stress in the circumferential direction caused by the impacts. The conventional SFRM, when strongly bonded with the steel, disintegrates through development of large millimeter-sized radial cracks and delamination within the SFRM parallel to the steel-SFRM interface.

FR-ECC specimen survived all 12 successive impacts without loss of material integrity. After the first impact,

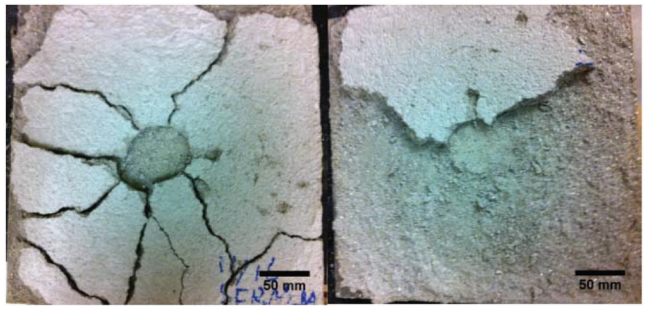

(a) SFRM Specimen after 6 impacts

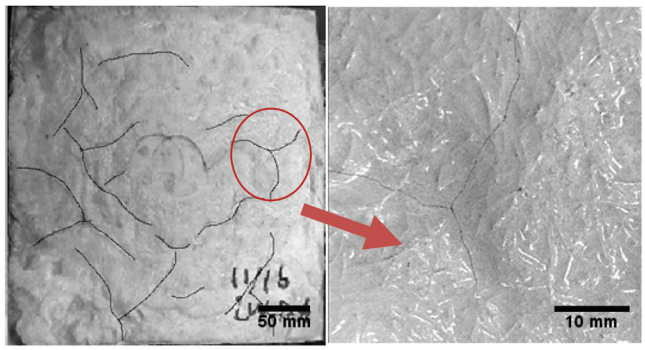

(b) FR-ECC specimen after 12 impacts

Fig. 7—Damage condition of FR-ECC and SFRM panel specimens after impacts. (Note: left image in (b) shows overall crack pattern. Right image shows enlarged microcracks in circle in left image; 1 mm = 0.0394 in.)

minor debonding of the ECC-steel interface at the edge was observed (Fig. A5 in the Appendix). After six impacts, microcracks began to appear in the ECC specimen, and gradually increased in length thereafter. Figure 7(b) shows the final crack pattern after all 12 impacts. Although slight debonding at the steel-FR-ECC interface was observed at the edge and corners, the use of bonding agent kept most of the interface intact and bonded. In the FR-ECC specimen, the impact energy is mainly dissipated through the development of micro-sized multiple cracks distributed over the volume of material. During the microcracking process, the fibers bridging the cracks partially debond and slip against the matrix, which

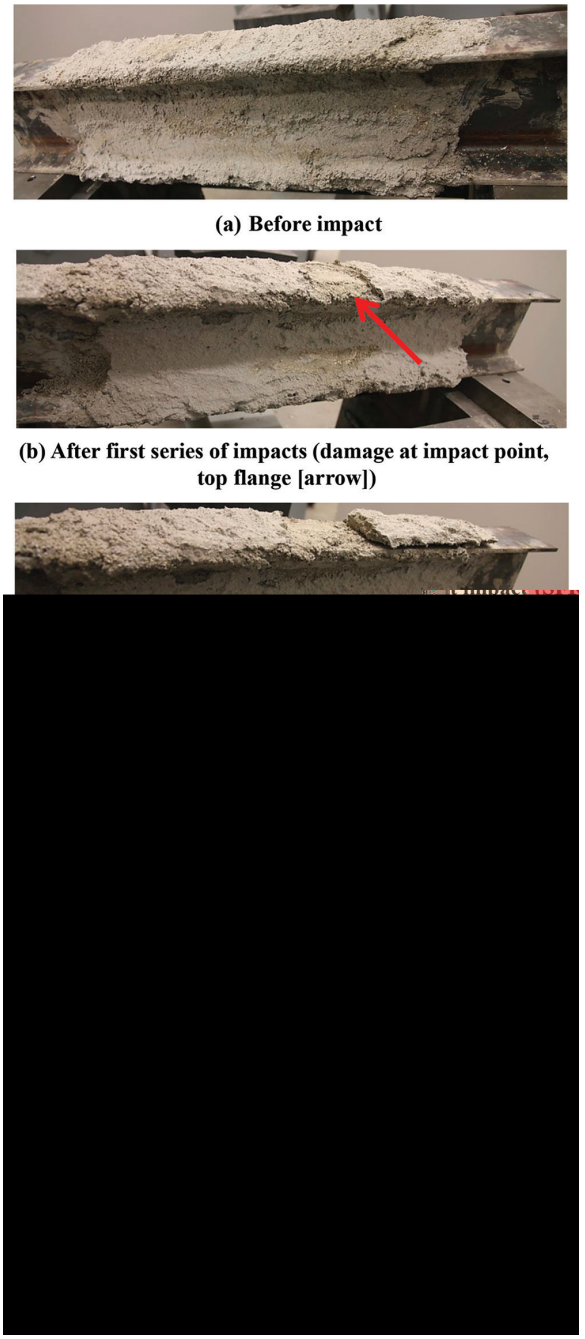

(a) Before impact

(b) After first series of impacts (damage at impact point, top flange [arrow])

Fig. 8—Condition of SFRM-protected steel beam before and after impacts.

dissipates the impact energy at the fiber-matrix interface, and prevents catastrophic failure of the FR-ECC insulation.

These impact test results show that even with the enforced strong bonding with the steel substrate, the cohesive strength is still a bottleneck for conventional SFRM, which prevents it from resisting the impact loads. In contrast, for FR-ECC, the high tensile strength and ductility ensure high cohesive strength and deformation compatibility with the steel substrate, which allow the FR-ECC insulation to take repeated impacts without failure.

Wrapped-around durability

Very different behavior of the SFRM and FR-ECC protected beam were observed during the impact tests on wrapped-around specimens.

Significant loss of the insulation layer in the SFRM protected beam was observed after the second series of impacts, particularly around the disk-shape impact head. After four series of impacts, most of the insulation material was detached, leaving the steel beam almost bare, as shown in Fig. 8. The detachment of the insulation layer initiated in the flange region, and later extended to the web region of the steel beam. It was observed that the insulation material detached piece by piece, which indicates that the material remaining on the steel beam exerted no restraint on the adjacent falling piece, and the insulation was attached to the substrate mainly due to adhesion at the interface. For such a material system, adhesion is necessary, and adhesive failure could lead to ultimate failure. The wrapped-around concept is not valid in conventional SFRM due to the poor cohesion within the material.

In the beam wrapped around by FR-ECC, shown in Fig. 9, no major damage was observed in the first three series of impacts. Instead, the impact head left a disk-shape indent on the FR-ECC. Slight damage on the edge of the flange was observed after the fourth series of impacts. The damage was located at the edge of the beam flange, where the steel beam imposed shear force on the FR-ECC layer due to the vibration caused by impact. The integrity of the FR-ECC layer, however, was still maintained. These test results show that despite zero bonding deliberately introduced in this experiment, the high cohesion and deformation capacity of the wrapped-around FR-ECC fireproofing system provides an additional mechanism (beyond the normal adhesion between FR-ECC and steel) to keep the insulation material in place, thereby improving impact resistance and durability of the insulation layer.

It is also observed that the FR-ECC protected steel beam can resist eccentric impact without catastrophic failure. In addition to the aforementioned impacts, an additional impact using 8.9 kg (19.6 lb) weight dropped from 112 cm (44 in.) height was applied at the edge of the beam where the insulation is not fully supported by the beam. Cracks in FR-ECC formed at the edge of the flange along with multiple microcracks in the middle of the upper flange due to bending effects, as shown in Fig. 10. In spite of this, local and overall material integrity was still maintained under such eccentric loading, which indicates that FR-ECC can potentially withstand various accidental impacts without major loss of insulation functionality.

CONCLUSIONS

In this feasibility study, a preliminary FR-ECC material using a large volume fraction of micro-sized hollow glass bubbles was investigated for its thermal and mechanical performance. The cohesive performance of FR-ECC insulation was characterized under impact load, and the concept of wrapped-around durability was also evaluated through impact tests. Based on the results of this experimental investigation, the following conclusions are drawn:

(a) Before impacts

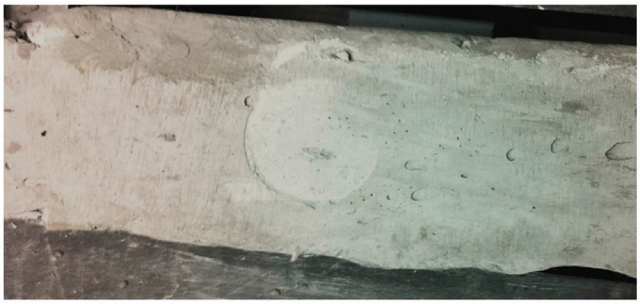

(b) After third series of impacts (indent of impact head on FR-ECC on top flange)

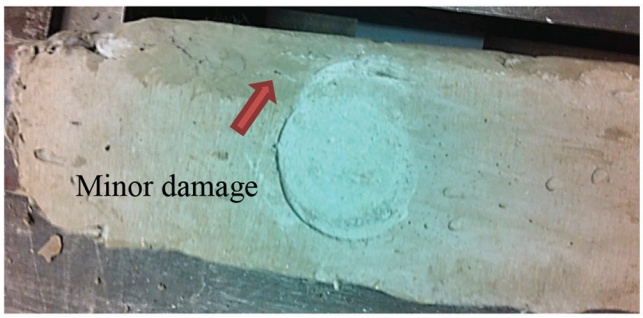

(c) After fourth series of impacts (further indent of impact head, with minor damage adjacent to impact point: no damage of FR-ECC on web)

Fig. 9—Condition of FR-ECC protected steel beam before and after impacts.

1. The feasibility of developing an FR-ECC with good thermal insulation property and durability, facilitated by high tensile strength (relative to SFRM) and high tensile ductility, was demonstrated experimentally. The new FR-ECC has a thermal insulation property comparable to current SFRM, but with tensile ductility at least two orders of magnitude higher than SFRM.
2. High tensile strength and damage tolerance of FR-ECC greatly improves the cohesion of the FR-ECC insulation system over conventional SFRM, and helps to maintain material integrity, even under severe loadings. Microcrack formation helps to dissipate the energy induced by impact loading without catastrophic failure.
3. The wrapped-around concept is experimentally demonstrated to be feasible. FR-ECC insulation systems can withstand impact load, even without the presence of adhesion at the steel-FR-ECC interface, which is impossible for the SFRM insulation system.

Fig. 10—Damage condition of FR-ECC protected steel beam after eccentric impact.

This study shows that FR-ECC with good mechanical performance and suitable thermal property has the potential to overcome the current durability issue of conventional SFRM and improve the overall fire resistance of a steel structure. This study only presents preliminary test results of the proposed FR-ECC material, and further development of this material, particularly in terms of spray-ability, is needed for field applications. In addition, large-scale structural fire tests and simulation analyses are necessary to fully evaluate the potential of FR-ECC.

AUTHOR BIOS

ACI member **Qian Zhang** *is a Graduate Student Research Assistant in the Department of Civil and Environmental Engineering (CEE) at the University of Michigan, Ann Arbor, MI. She received her BS in civil engineering from Tsinghua University, Beijing, China, and her MSE in civil engineering (structures) from the University of Michigan. Her research interests include the development of advanced cementitious composites for fire and high-temperature applications.*

ACI member **Ravi Ranade** *is a Postdoctoral Research Fellow in the CEE Department at the University of Michigan. He received his BS in civil engineering from the Indian Institute of Technology, Mumbai, India, and his MSE and PhD in civil engineering (structures and materials) from the University of Michigan. His research interests include the development of advanced cementitious composites for resilient and sustainable infrastructure systems.*

Victor C. Li, *FACI, is the E. B. Wylie Professor in the CEE Department at the University of Michigan. His research interests include the micromechanics and design of ultra-ductile and green cementitious composites, their application to innovative and sustainable infrastructure systems, and integration of materials and structural design.*

ACKNOWLEDGMENTS

The authors wish to express their gratitude and sincere appreciation to 3M (glass bubbles), Lafarge (cement), W. R. Grace (SP and VMA), and Kuraray (PVA fiber) for supplying materials for this research project. The authors are also grateful to R. Laine and N. Taylor for their assistance in thermal gravimetric analysis.

REFERENCES

1. NIST GCR 04-872, "Fire Protection of Structural Steel in High-Rise Buildings," National Institute of Standards and Technology, Gaithersburg, MD, 2004, 88 pp.

2. NIST NCSTAR 1, "Collapse of the World Trade Center Towers Final Report: Federal Building and Fire Safety Investigation of the WTC Disaster," National Institute of Standards and Technology, Gaithersburg, MD, 2005, 298 pp.

3. Carino, N. J.; Starnes, M. A.; Gross, J. L.; Yang, J. C.; Kukuck, S. R.; Prasad, K. R.; and Bukowski, R. W., "Passive Fire Protection," *Federal Building and Fire Safety Investigation of the World Trade Center Disaster* NIST NCSTAR 1-6A, National Institute of Standards and Technology, Gaithersburg, MD, 2005, 326 pp.

4. Braxtan, N. L., and Pessiki, S. P., "Bond Performance of SFRM on Steel Plates Subjected to Tensile Yielding," *Journal of Fire Protection Engineering*, V. 21, No. 1, Feb. 2011, pp. 37-55.

5. Braxtan, N. L., and Pessiki, S. P., "Postearthquake Fire Performance of Sprayed Fire-Resistive Material on Steel Moment Frames," *Journal of Structural Engineering*, ASCE, V. 137, 2011, pp. 946-953.

6. Pessiki, S.; Kwon, K.; and Lee, B., "Fire Load Behavior of Steel Building Columns With Damaged Spray-Applied Fire Resistive Material," *Proceedings of 4th International Workshop on Structures in Fire*, Aveiro, Portugal, 2006, pp. 235-245.

7. Tomecek, D. V., and Milke, J. A., "A Study of the Effect of Partial Loss of Protection on the Fire Resistance of Steel Columns," *Fire Technology*, V. 29, No. 1, 1993, pp. 4-21.

8. Keller, W. J., and Pessiki, S., "Effect of Earthquake-Induced Damage to Spray-Applied Fire-Resistive Insulation on the Response of Steel Moment-Frame Beam-Column Connections during Fire Exposure," *Journal of Fire Protection Engineering*, V. 22, No. 4, 2012, pp. 271-299.

9. Li, G., and Kodur, V., "Role of Insulation Effectiveness on Fire Resistance of Steel Structures under Extreme Loading Events," *Journal of Performance of Constructed Facilities*, V. 25, No. 4, 2011, pp. 277-286.

10. Li, V. C.; Wang, S.; and Wu, C., "Tensile Strain-Hardening Behavior of PVA-ECC," *ACI Materials Journal*, V. 98, No. 6, Nov.-Dec. 2001, pp. 483-492.

11. Kanda, T., and Li, V. C., "A New Micromechanics Design Theory for Pseudo Strain Hardening Cementitious Composite," *Journal of Engineering Mechanics*, ASCE, V. 125, No. 4, 1999, pp. 373-381.

12. Li, V. C., and Leung, C. K. Y., "Steady-State and Multiple Cracking of Short Random Fiber Composites," *Journal of Engineering Mechanics*, V. 118, No. 11, 1992, pp. 2246-2264.

13. Li, V. C., "Engineered Cementitious Composites—Tailored Composites through Micromechanical Modeling," *Fiber Reinforced Concrete: Present and the Future*, N. Banthia, A. A. Bentur, and A. Mufti, eds., Canadian Society for Civil Engineering, Montreal, QC, Canada, 1998, pp. 64-97.

14. Li, V. C.; Wu, C.; Wang, S.; Ogawa, A.; and Saito, T., "Interface Tailoring for Strain-Hardening Polyvinyl Alcohol-Engineered Cementitious Composites (PVA-ECC)," *ACI Materials Journal*, V. 99, No. 5, Sept.-Oct. 2002, pp. 463-472.

15. Wang, S., and Li, V. C., "Materials Design of Lightweight PVA-ECC," *Proceedings of HPFRCC*, A. E. Naaman and H. W. Reinhardt, eds., Ann Arbor, MI, 2003, pp. 379-390.

16. Kim, Y. Y.; Kong, H. J.; and Li, V. C., "Design of Engineered Cementitious Composite (ECC) Suitable for Wet-mix Shotcreting," *ACI Materials Journal*, V. 100, No. 6, Nov.-Dec. 2003, pp. 511-518.

17. Yang, E., and Li, V. C., "Rate Dependence in Engineered Cementitious Composites," *Proceedings of International RILEM Workshop HPFRCC in Structural Applications*, RILEM SARL, Honolulu, HI, 2006, pp. 83-92.

18. Magalhães, M. S.; Toledo Filho, R. D.; and Fairbairn, E. M. R., "Thermal Properties and Resistance to Thermal Shock of Strain Hardening Cement-Based Composites," *Proceedings of 2nd International RILEM Conference on SHCC*, Rio de Janeiro, Brazil, 2011, pp. 189-198.

19. Sahmaran, M.; Lachemi, M.; and Li, V. C., "Assessing the Mechanical Properties and Microstructure of Fire-Damaged Engineered Cementitious Composites," *ACI Materials Journal*, V. 107, No. 3, May-June 2010, pp. 297-304.

20. ASTM E2584-07, "Standard Practice for Thermal Conductivity of Materials Using a Thermal Capacitance (Slug) Calorimeter," ASTM International, West Conshohocken, PA, 2007, 9 pp.

21. Russell, H. W., "Principles of Heat Flow in Porous Insulators," *Journal of the American Ceramic Society*, V. 18, 1935, pp. 1-5.

22. Loeb, A. L., "Thermal Conductivity: VIII, A Theory of Thermal Conductivity of Porous Materials," *Journal of the American Ceramic Society*, V. 37, 1954, pp. 96-99.

23. Laurent, J. P., "An Estimation Model for the Dry Thermal-Conductivity of Autoclaved Aerated Concrete," *Materials and Structures*, V. 24, 1991, pp. 221-226.

24. Kunii, D., and Smith, J. M., "Heat Transfer Characteristics of Porous Rocks," *AIChE Journal*, American Institute of Chemical Engineers, V. 6, No. 71, 1960, pp. 71-78.

25. Bouguerra, A.; Ledhem, A.; de Barquin, F.; Dheilly, R. M.; and Queneudec, M., "Effect of Microstructure on the Mechanical and Thermal Properties of Lightweight Concrete Prepared From Clay, Cement, and Wood Aggregate," *Journal of Cement and Concrete Research*, V. 28, No. 8, 1998, pp. 1179-1190.

26. Dos Santos, W. N., "Effect of Moisture and Porosity on the Thermal Properties of A Conventional Refractory Concrete," *Journal of the European Ceramic Society*, V. 23, No. 5, 2003, pp. 745-755.

27. Lu-shu, K.; Man-qing, S.; Xing-Sheng, S.; and Yun-xiu, L., "Research on Several Physico-Mechanical Properties of Lightweight Aggregate Concrete," *International Journal of Lightweight Concrete*, V. 2, No. 4, 1980, pp. 185-191.

28. Akman, M. S., and Tasdemir, M. A., "Tasiyici Malzeme Olarak Perlit Betonu (Perlite Concrete as a Structural Material)," *1st National Perlite Congress*, Ankara, Turkey, 1977, pp. 40-48.

29. Blanco, F.; Garcia, P.; Mateos, P.; and Ayala, J., "Characteristics and Properties of Lightweight Concrete Manufactured With Cenospheres," *Journal of Cement and Concrete Research*, V. 30, 2000, pp. 1715-1722.

30. Bave, G., "Aerated Light-Weight Concrete—Current Technology," *Proceedings of the 2nd International Symposium on Light-weight Concretes*, London, UK, 1980, pp. 28-35.

31. Marshall, D. B., and Cox, B. N., "A J-Integral Method for Calculating Steady-State Matrix Cracking Stresses in Composites," *Mechanics of Materials*, V. 7, No. 2, 1988, pp. 127-133.

32. Griffith, A. A., "The Phenomena of Rupture and Flow in Solids," *Philosophical Transactions of the Royal Society of London*, V. 221, 1921, pp. 163-198.

33. Kanda, T., and Li, V. C., "Multiple Cracking Sequence and Saturation in Fiber Reinforced Cementitious Composites," *Concrete Research and Technology*, V. 9, No. 2, 1998, pp. 19-33.

34. ASTM C109/C109M-02, "Standard Test Method for Compressive Strength of Hydraulic Cement Mortars (Using 2-in. or [50-mm] Cube Specimens)," ASTM International, West Conshohocken, PA, 2002, 6 pp.

35. Concrete Engineering Series 82, "Recommendations for Design and Construction of High. Performance Fiber Reinforced Cement Composites with Multiple Fine Cracks (HPFRCC)," Japan Society of Civil Engineers, Tokyo, Japan, Mar. 2008, 113 pp.

36. ASTM E1269-11, "Standard Test Method for Determining Specific Heat Capacity by Differential Scanning Calorimetry," ASTM International, West Conshohocken, PA, 2011, 6 pp.

37. AC377, "Acceptance Criteria for Spray-Applied and Intumescent Mastic Coating Fire-Protection Materials," International Code Council—Evaluation Service, July 2004, 20 pp.

38. Unified Facilities Guide Specifications Division 7, "Spray-Applied Fireproofing (Section 07 81 00)," prepared by U.S. Army Corps of Engineers, Washington, DC, Aug. 2002, 16 pp.

39. ASTM E605-93(06), "Standard Test Methods for Thickness and Density of SFRM Applied to Structural Members," ASTM International, West Conshohocken, PA, 2006, 6 pp.

40. Li, M., and Li, V. C., "Influence of Material Ductility on the Performance of Concrete Repair," *ACI Materials Journal*, V. 106, No. 5, Sept.-Oct. 2009, pp. 419-428.

41. Bentz, D. P., "Combination of Transient Plane Source and Slug Calorimeter Measurements to Estimate Thermal Properties of FRM," *ASTM Journal of Testing and Evaluation*, V. 35, No. 3, 2007, pp. 240-244.